applied sciences

MDPI

Article

Simulation Research on the Grouser Effect of a Reconfigurable Wheel-Crawler Integrated Walking Mechanism Based on the Surface Response Method

Pengfei Zhou [1,2], Shufeng Tang [1,2,*] and Zaiyong Sun [1]

[1] Science College, Inner Mongolia University of Technology, Hohhot 010051, China
[2] Inner Mongolia Key Laboratory of Special Service Intelligent Robotics, Hohhot 010051, China
* Correspondence: tangshufeng@imut.edu.cn

Featured Application: The reconfigurable wheel-crawler walking mechanism involved in this study is a type of walking mechanism which can manage a high moving speed and good terrain adaptability given the unstructured terrain existing in the Qinghai–Tibet Plateau's scientific research station. The mechanism can achieve the purpose of switching between circular tire mode and triangular crawler mode without changing the working parts through the integration of wheeled and tracked components. In this study, the grouser effect of the walking mechanism was analyzed, and the parameters with the largest traction force were obtained, which can guide the machining of a prototype of the reconfigurable wheel-shoe integrated walking mechanism.

Abstract: To improve the unstructured terrain traversing performance of the scientific research robot of the Qinghai–Tibet Plateau station, the parameters of the track shoe of the reconfigurable wheel-crawler walking mechanism were studied. Based on a typical track shoe puncture effect model, the experimental design was carried out based on the surface response method, and the dynamic model of the triangular crawler mode of the reconfigurable wheel-crawler walking mechanism was constructed and tested using RecurDyn V9R3 software. Through an analysis of the simulation results, the interaction of the grouser parameters was further clarified, and the regression equation of the traction force of the walking mechanism was obtained. The grouser parameters that enabled the reconfigurable wheel-crawler walking mechanism to have the maximum traction were obtained; these will be used to guide the machining of the prototype walking mechanism.

Keywords: wheel-crawler integration; grouser effect; surface response method; RecurDyn; walking mechanism

Citation: Zhou, P.; Tang, S.; Sun, Z. Simulation Research on the Grouser Effect of a Reconfigurable Wheel-Crawler Integrated Walking Mechanism Based on the Surface Response Method. *Appl. Sci.* **2023**, *13*, 4202. https://doi.org/10.3390/app13074202

Academic Editors: Giovanni Boschetti and João Miguel da Costa Sousa

Received: 4 February 2023
Revised: 16 March 2023
Accepted: 20 March 2023
Published: 26 March 2023

1. Introduction

Due to the harsh climate and extreme environment on the Qinghai-Tibet Plateau, humanized scientific research activities are facing great difficulties, and the depth and breadth of scientific research are greatly limited. It has also become important for robot technology research to replace manual scientific research tasks and patrol the scientific research station. In the process of carrying out scientific research and inspection tasks, the scientific research robots of the Qinghai–Tibet Plateau research station need to pass through complex and unpredictable terrain where cement roads, wetlands, gravel, sand, snow, ice, grassland, muddy land, and steep slopes coexist. Because the adaptability of the robot to the terrain is not only related to the driving force of the walking mechanism but is also closely related to the interaction between the walking mechanism and the ground, it is necessary to study the interaction between the walking mechanism and the ground while studying a walking mechanism with excellent adaptability to unstructured terrain, to further improve the terrain traversing performance of the walking mechanism [1].

Ground mechanics gradually attracted people's attention with the appearance of tractors, and in 1913, R. Bernstein of Germany put forward an expression of the relationship between the subsidence depth of passive wheels and their grounding pressure. With the deepening of the research, the American scholar Bekker published two monographs entitled Driving Principles of Road Vehicles [2] and Driving Off-road [3] in 1956 and 1960, respectively. After more than 100 years of development, the area of ground mechanics has been studied further, and its research methods can be summarized as the purely empirical method, the semi-empirical method, the model test method, and the numerical analysis [4]. The pure empirical method is an empirical model established entirely by experimental data, represented by the mobile performance model of an agricultural vehicle's bias tire built by Wismer. The model includes the wheel torque, speed, traction, soil strength, the tire section width, the tire's diameter, and other parameters [5]. Although the model is simple and practical, it can only be applied to situations similar to the soil environment obtained by this formula, which has great limitations [6]. The semi-empirical method is represented by the pressure–settlement relationship proposed by Bekker [7], which is a mechanical model of the ground based on the Coulomb criterion of soil failure related to thrust obtained by measuring the mechanical characteristics of the ground through experiments. The model test method is the soil tank test method, which is a research method of reducing the model in equal proportions, testing it in a laboratory soil tank, and then redrawing the prototype's structure. Liang Ding and others used the model test method to analyze the physical effects of wheel lugs, sliding and sinking, wheel size and load, and finally deduced the mechanical model for predicting the behavior of a rigid wheel of a planetary wheeled mobile robot driving in sand [8,9]. A soil trough test is more economical than a prototype test, but it cannot solve the related problems of micro-local phenomena. Since the 1960s, numerical simulation methods have been gradually applied to the study of ground mechanics, among which, the finite element method and the discrete element method are important research methods [1]. To study the influence of thrust, water content, the shear rate, and the structural parameters of a track shoe on soft ground, Yang Congbin et al. established a finite element model of an eight-tooth mechanism on soft ground and conducted a traction test [10–12]. Akira Yokoyama et al. studied the influence of the open space between the tracks on the total traction by using a quasi-two-dimensional track shoe model and the discrete element method [13]. Li Jun et al. used the Mckyes–Ali three-dimensional model to analyze the interaction between the baffle and the soil; compared the predicted results, Baker's model, and the measured values; and found that the predicted values obtained by the three-dimensional model were closer to the measured values [14,15].

As an important branch of ground mechanics, the mechanical characteristics of the interaction between a crawler-type walking mechanism and the ground have also been studied by many scholars. The resulting force of the ground acting on the crawler is called the traction force of the crawler robot, and the traction force and the ground shear force are a pair of interactive forces, so the traction force is closely related to the ground adhesion performance of the crawler [16]. The additional traction of the tracked robot caused by the action of the grouser is called the grouser effect, and parameters such as the width, length, height, and shape of the tread shoes influence the adhesion between the track and the ground. To better evaluate the traction and running performance of a four-track mining vehicle, Zhiyong Xu proposed a dynamic subsidence phenomenon involving a soft seabed as well as front and rear track effects and established mathematical models of the subsidence and the traction–slip rate based on the theory of topographic mechanics [17]. Congbing Yang et al. divided the soil thrust of the track shoe into the force acting on the bottom of the track shoe, the force perpendicular to the shear plane of the track shoe, and the force acting on both ends of the track shoe, then deduced them and verified the new thrust formula through a traction test of the actual track shoe [18]. To further optimize the walking mechanism of a tracked vehicle, Lijun Zheng et al. conducted a traction test on a simulated track shoe in a soil trough in the laboratory and found a variation in the law of traction performance under different parameters by changing the structural parameters of the track shoe [19]. Zeren Chen et al. established the gravel pavement model and the virtual prototype model of an electric shovel based on the discrete element method. On this basis, through coupling DEM and multi-body dynamics, the effects of pre-tightening, wheel spacing, sprocket speed, and the track's tooth height on the performance of tracked chassis were discussed [20]. Linxuan Zhou and others put forward a systematic and accurate method of discrete element modeling for sand pavements. Based on the mechanical parameters measured by mechanical tests of the soil, the sand was modeled; on this basis, the discrete element model of the track–sand interaction was established. The track model at different speeds was numerically simulated, and the simulation results were compared with the results of an indoor soil trough test [21]. Yang et al. designed a sand track shoe based on the sand traversing mechanism of ostrich feet. With the structural parameters of this kind of track shoe as the research object, the mathematical model of the track shoe–sand traction force was established based on the theory of soil mechanics, and finite element analysis of different forms of track shoes moving on sand was carried out by combining this with the orthogonal experimental method [22].

With the continual development of computer technology, the finite element method has been more widely used in studies of the interaction between a track shoe and the ground. This method can quickly and conveniently study the influence of different driving conditions, soil parameters, parameters of track shoe structure, and other factors on traction performance [16]. The surface response method is a statistical method used to find the optimal value in a certain range, which can fit the complex unknown functional relationship with a simple linear or quadratic polynomial model in a small area [23]. In this study, based on the model of the grouser effect, the surface response method was used to construct the test, and the finite element analysis method was used to simulate it. Through screening and analysis of the simulation results, the regression equation of the grouser effect was constructed, and the treading parameters that enable the reconfigurable wheel-crawler walking mechanism to achieve maximum traction were determined under this guidance. This parameter will be used to guide the machining of a prototype of a reconfigurable wheel-crawler walking mechanism.

The structure of this study was as follows. The second part included a structural analysis of the reconfigurable wheel-crawler integrated walking mechanism designed to adapt to the unstructured terrain in the Qinghai–Tibet Plateau's scientific research station. In the third part, the interaction between typical T-shaped, π-shaped, V-shaped, and K-shaped track shoes and the ground is analyzed, and the model of the grouser effect was constructed. In the fourth part, to determine the controllable factors of the grouser effect, a surface response test design was carried out, and the dynamic model of the reconfigurable wheel-crawler walking mechanism in the triangular crawler mode was constructed by RecurDyn for the simulation test. In the fifth part, the regression equation of the traction force of the walking mechanism was obtained by judging and analyzing the experimental data, and a coupling analysis of multiple factors of the grouser was carried out. Finally, the parameters of the grouser that can enable the reconfigurable wheel-crawler walking mechanism to obtain the maximum traction force were obtained. The last section of this article is dedicated to the conclusions of the study.

2. Structural Analysis of the Reconfigurable Wheel-Crawler Integrated Walking Mechanism

The complex and unpredictable terrain of cement roads, wetlands, gravel, snow, ice, grassland, muddy land, steep slopes, and steps in the Qinghai-Tibet Plateau Namco Research Station requires the walking mechanism of the scientific research robot to have high mobility. The wheel base of the robot is 750 mm, the wheel base is 540 mm, the height of the chassis from the ground is not less than 170 mm, the robot load is 25 kg, and it can adapt to the above, unstructured terrain environment. The maximum moving speed is 3 km/h, the maximum climbing angle is 30°, the maximum width across ravines is 300 mm, and the obstacle clearance height is not less than 150 mm. According to the above requirements, the robot's walking mechanism not only needs to have a fast-moving speed but also a good ability to traverse unstructured terrain. Through a comparison of the performance and structures of wheeled, tracked, and wheel-crawler combined walking mechanisms, a design scheme for a reconfigurable wheel-crawler integrated walking mechanism was proposed here.

The reconfigurable wheel-crawler integrated walking mechanism designed in this study is modular, the reconfigurability of which is composed of a rotary driving system, a deformation positioning system, a deformation linkage system, and three sets of swing arm systems, as shown in Figure 1. The rotary driving system mainly consists of a driving motor, a gear set, a hollow shaft, tooth gears, and a belt wheel. To further improve the level of its modularity, the driving motor has an inverted design, which is built into the hollow shaft, passing the torque to the hollow shaft through the gear set and then outputting the driving torque through the hollow shaft. The re-configurable framework consists of a deformation positioning system, a deformation linkage system, and the swing arm system, including a positioning motor, a locking gear, a push rod, a thrust ring, a sliding ring, a small link rod, a bracket, a belt wheel, a drive shaft, a swing arm and a crawler belt outside the swing arm.

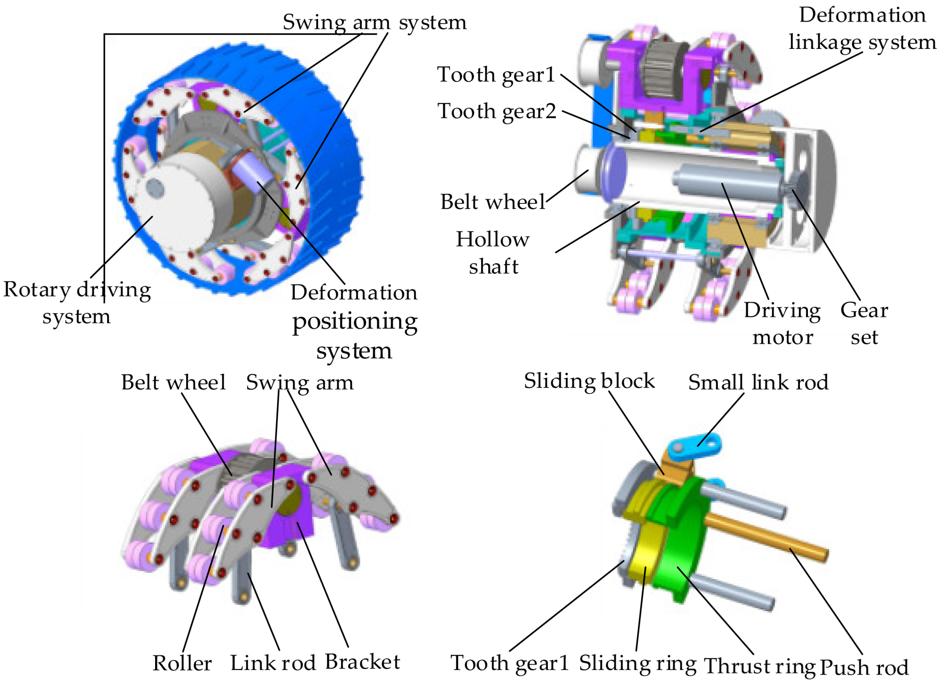

Figure 1. Structural diagram of the reconfigurable wheel-crawler robot.

The reconfigurable wheel-crawler integrated walking mechanism achieves the purpose of switching between circular wheel mode and triangular crawler mode without changing the working parts through the integration of the components of the wheel and track configurations, as shown in Figure 2, relevant videos are provided in the Supplementary Materials. When passing across a flat road, the robot can move quickly and cross obstacles effectively by switching to the circular tire mode. When passing through unstructured terrains such as sand, snow, and muddy roads, the robot can pass through a variety of terrain types smoothly by switching to the triangular crawler mode. At the same time, the length of the track is basically unchanged in the two modes (the wheel and the triangular crawler), which effectively reduces the requirements for the elastic deformation performance of the track and reduces the wear of the track.

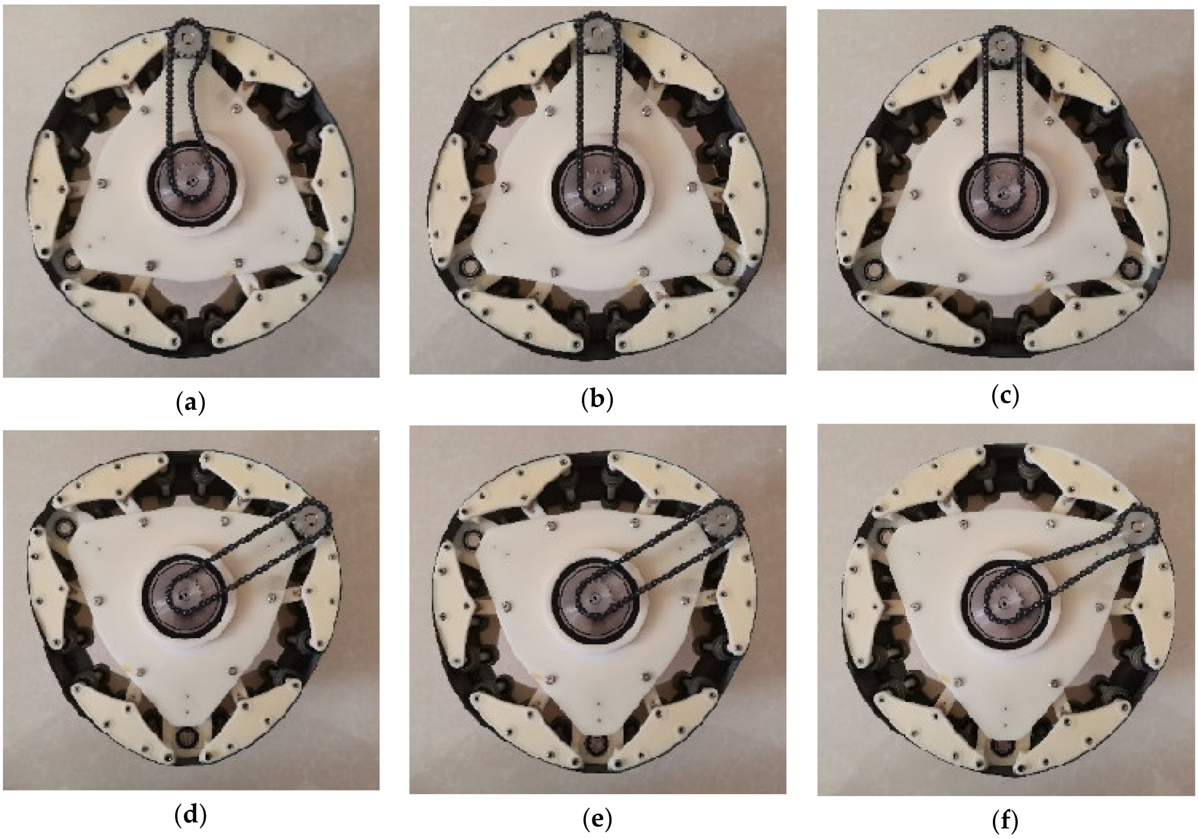

Figure 2. The process of switching to the walking mode of the reconfigurable wheel-crawler integrated mechanism. (**a**) The circular wheel mode; (**b**) the swing arm is recovered, and the traveling mechanism is switched from the circular wheel mode to the triangular crawler mode; (**c**) the triangular crawler mode; (**d**) the triangular crawler mode with the bracket is below; (**e**) the process of changing from the triangular crawler mode to the circular wheel mode, with the bracket is retracting, the swing arm is expanding; (**f**) the circular wheel mode after the mode switched.

As the key component of the reconfigurable wheel-crawler integrated walking mechanism in contact with the ground, the crawler that is wrapped on the outside of the walking mechanism plays an important role in the interaction force and the transmission of torque between the walking mechanism and the ground. The triangular crawler mode is the main mode of the reconfigurable wheel-crawler integrated walking mechanism passing through unstructured terrain, and the structure of the crawler, especially the parameters of the grouser, has a strong influence on its tractability. To improve the trafficability of the walking mechanism on unstructured terrain, it is necessary to conduct further research on the grouser effect.

3. Theoretical Analysis of the Grouser Effect

3.1. Relationship between the Vertical Load and Subsidence of the Grouser

At present, the more common track shoe shapes can be roughly summarized as T-shapes, π-shapes, V-shapes, and K-shapes, as shown in Figure 3 [12]. In the L-shaped track shoe shown in Figure 4a, l is the pitch of the track shoe; d and h are the width and thickness of the grouser, respectively, where $d = \lambda l$ and λ is the ratio of the thickness of the grouser to the pitch of the track shoe; i is the shear displacement of the track shoe; z is the sinking displacement of the track shoe; p_1 is the unit of pressure of the ground acting on the track shoe; p_2 is the unit of pressure of the soil acting on the unit of pressure of the track shoe's thickness; and F_{max} is the maximum tractive force produced by the soil.

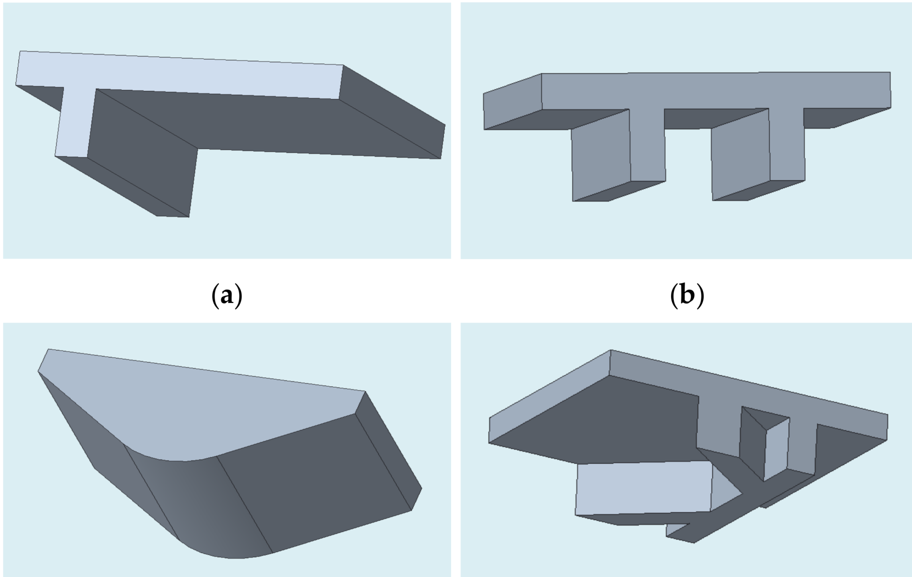

(a) (b) (c) (d)

Figure 3. The more common track shoe shapes are as follows: (**a**) T-shape track shoe; (**b**) π-shape track shoe; (**c**) V-shape track shoe; (**d**) K-shape track shoe.

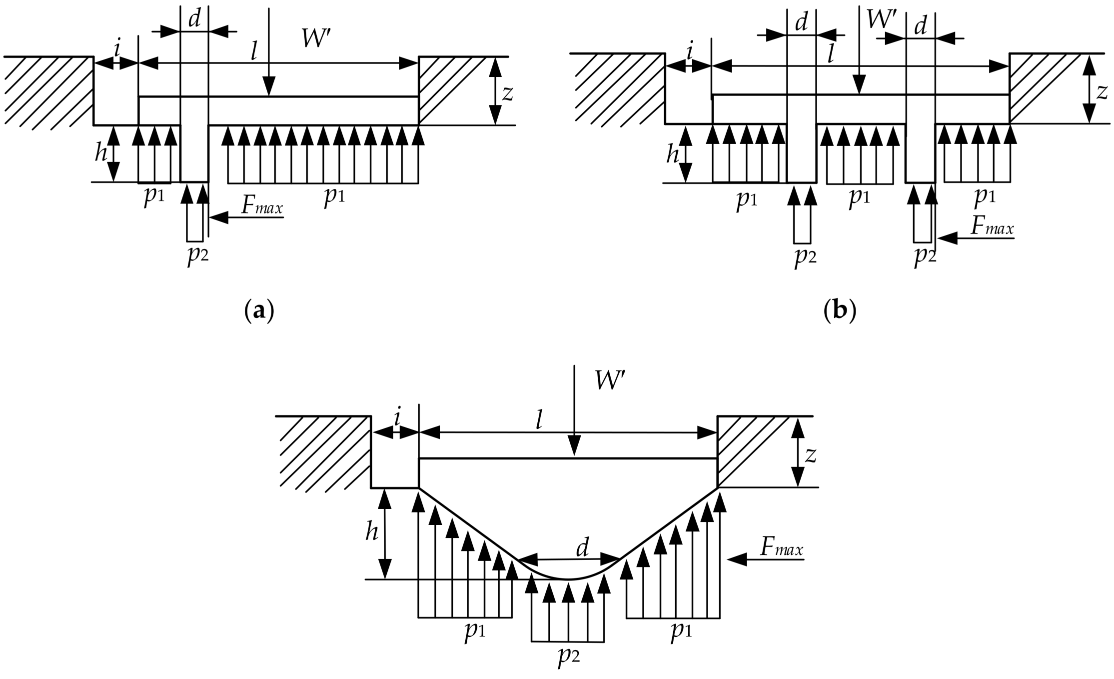

Figure 4. Schematic diagram of the interaction force between the track shoe and the soil. (**a**) Schematic diagram of the interaction force between an L-shaped track shoe and the soil. (**b**) Schematic diagram of the interaction force between a π-shaped track shoe and the soil. (**c**) Schematic diagram of the interaction force between a V-shaped track shoe and the soil.

According to Beck's pressure-subsidence relationship formula,

$$p = \left(\frac{k_c}{b} + k_\varphi\right) z^n$$

where k_c is the coefficient of soil cohesion, k_φ is the coefficient of the soil's internal friction angle, z is the amount of soil subsidence and n is the soil deformation index.

It can be found that the unit of pressure p_1 of the ground acting on the track shoe and the unit of pressure p_2 of the soil acting on the grouser are the following, respectively.

$$p_1 = \left(\frac{k_c}{b} + k_\varphi\right) z^n \tag{1}$$

$$p_2 = \left(\frac{k_c}{b} + k_\varphi\right) (z+h)^n \tag{2}$$

Since the track shoe is balanced in the vertical direction, it can be found that

$$W' = p_1(1-\lambda)lb + p_2\lambda lb \tag{3}$$

$$W' = \frac{l}{L} W$$

where b is the width of the track, W is the load of the traveling mechanism, L is the length of the track on the ground and W' is the force acting on a single track shoe.

By substituting Equations (1) and (2) into Equation (3), we can obtain:

$$W' = lb\left(\frac{k_c}{b} + k_\varphi\right)\left[(h+z)^n\lambda + z^n(1-\lambda)\right] \tag{4}$$

For the π-shaped track shoe shown in Figure 4b, the total width of the grouser is $2d$, and its force balance formula in the vertical direction is

$$W' = lb\left(\frac{k_c}{b} + k_\varphi\right)\left[(h+z)^n 2\lambda + z^n(1-2\lambda)\right] \tag{5}$$

In the V-shaped track shoe shown in Figure 4c, the grouser's width can be equivalent to:

$$d' = d + \frac{l-d}{2} = \frac{d+l}{2}$$

The force balance formula in the vertical direction is

$$W' = \frac{lb}{2}\left(\frac{k_c}{b} + k_\varphi\right)\left[(h+z)^n(l+d) + z^n(l-d)\right] \tag{6}$$

In the K-shaped track shoe shown in Figure 5, the bottom area of the grouser is about

$$S_2 = 2\lambda l(b - w\sin\alpha)$$

The contact area of the track shoes with the ground is approximately

$$S_1 = bl - \lambda l(b - w\sin\alpha)$$

The force balance formula in the vertical direction is

$$W' = lb\left(\frac{k_c}{b} + k_\varphi\right)\left\{z^n[bl - \lambda l(b - w\sin\alpha)] + (z+h)^n[2\lambda l(b - w\sin\alpha)]\right\} \tag{7}$$

where α is the angle between the inclined grouser and the horizontal grouser ($\alpha \in [0^\circ, 90^\circ]$) and w is the equivalent length of the inclined grouser.

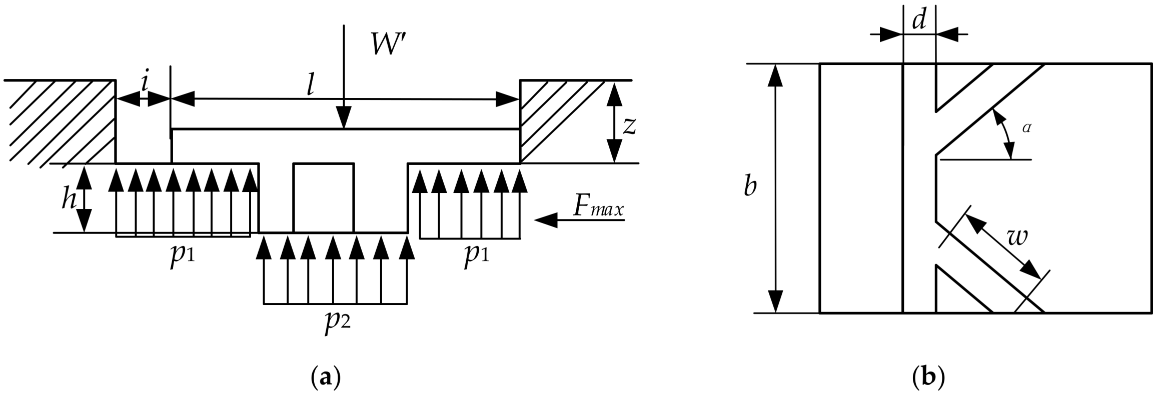

Figure 5. Schematic diagram of the interaction force between a K-shaped track shoe and the soil. (**a**) Side view of the force diagram of a K-shaped track shoe. (**b**) Dimension diagram of a K-shaped track shoe.

Through Equations (4)–(7), the force balance equation in the vertical direction of the track shoe can be summarized as

$$W' = b\left(\frac{k_c}{b} + k_\varphi\right)\left[z^n B_1 + (z+h)^n B_2\right] \tag{8}$$

where B_2 is the equivalent width of the grouser and B_1 is the width of the track shoe minus the width of the grouser.

According to Equation (8), the driving resistance caused by subsidence can be obtained as follows:

$$R = \frac{B_1}{l}\int_0^z p_1 dz + \frac{B_2}{l}\int_0^{z+h} p_2 dz \tag{9}$$

3.2. Calculation and Analysis of the Traction Force under the Grouser Effect

The traction force produced by the track shoe during the process of movement, that is, the reaction force received by the track shoe during the shearing process, can usually be divided into the vertical thrust F_1 acting on the surface of the track shoe, the force F_2 acting on the bottom of the grouser, the force F_3 acting on both sides of the track shoe and the grouser, and the force F_4 acting on the grouser. The shear stress of a single-track shoe on the ground is

$$F_0 = F_1 + F_2 + F_3 + F_4 \tag{10}$$

According to the Coulomb formula:

$$F_1 = B_1(c + p_1 \tan\varphi)\left(1 - e^{-i/k}\right) \tag{11}$$

$$F_2 = B_2(c + p_2 \tan\varphi)\left(1 - e^{-i/k}\right) \tag{12}$$

In Figure 6, the force acting on both sides of the track shoe can be regarded as a strip load on a semi-infinite body. Under the action of the strip load, p, the stress at any point in the semi-infinite body in the x direction is:

$$\delta_x = -\frac{p}{2\pi}\int_{\theta_1}^{\theta_2} \sin^2\theta d\theta$$

When $\theta_{1\,=}\,0$,

$$\delta_x = -\frac{p}{2\pi}(\pi - 2\theta - \sin 2\theta)$$

Moreover, because

$$\tan\theta = \frac{h}{b}$$

$$p = \frac{W\prime}{bl}$$

The force F_3 acting on both sides of the track shoe and the grouser is

$$F_3 = \frac{W'h}{b\pi}\arctan\left(\frac{h}{b}\right) \tag{13}$$

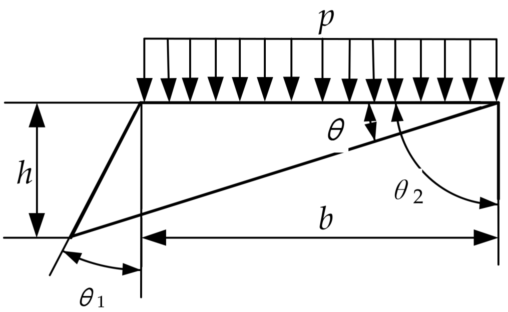

Figure 6. Stress distribution of the semi-infinite body under a band load.

The force F_4 acting on the spine was analyzed using the principle of a retaining wall, as shown in Figure 7. According to Rankine's earth pressure theory, under the action of a uniformly distributed load p on the track shoe, the passive ground pressure on the horizontal grouser is

$$\sigma = \gamma z N_\varphi + pN_\varphi + 2c\sqrt{N_\varphi}$$

where γ is the weight of the soil unit and N_φ is the flow value.

$$F_{41} = \int_0^h \sigma b dz = \frac{1}{2}\gamma h^2 b N_\varphi + phbN_\varphi + 2chb\sqrt{N_\varphi}$$

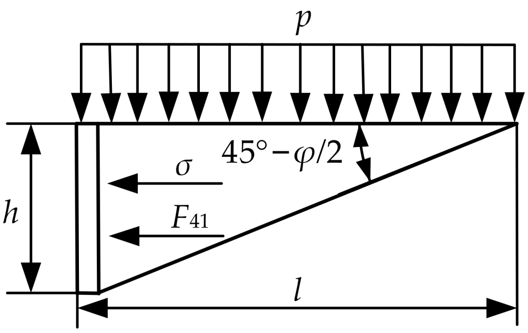

Figure 7. Schematic diagram of the force on the grouser.

In the K-shaped track shoe shown in Figure 5b, the passive ground pressure on a single inclined grouser is

$$F_{42} = \frac{1}{2}\gamma h^2 w \sin\alpha N_\varphi + phw\sin\alpha N_\varphi + 2chw\sin\alpha\sqrt{N_\varphi} + chw\cos\alpha$$

If we consider the four common track shoes in Figure 3 and compare their structural features comprehensively, the force F_4 acting on the grouser can be obtained as follows

$$F_4 = n_1 F_{41} + n_2 F_{42}$$

where n_1 is the number of horizontal grousers, n_1 can be 0 or 1; and n_2 is the number of inclined grousers, either 0 or 2. When n_1 = 1 and n_2 = 0, the force on the grouser of a T-shaped track, a π-shaped track, and a V-shaped track can be solved; when n_1 = 1 and n_2 = 2, the force on the grouser of a K-shaped track can be solved; and when n_1 = 0 and n_2 = 2, the force on the grouser of a figure-eight track can be solved.

From Equations (9) and (10), it can be seen that the traction force on a single-track shoe is

$$F = F_0 - R \tag{14}$$

4. Simulation Test of the Grouser Effect

The analysis in the previous section preliminarily clarified that the traction force of track shoes is not only related to the soil parameters but also the track shoe's width b, the track shoe's pitch l, the grouser's height h, the grouser's thickness λl, and the grouser's angle α. To further verify the implications of the previous section, an experimental design was carried out, and the parameters of the grouser for the optimal performance of the reconfigurable wheel-crawler walking mechanism were determined through simulation tests.

4.1. Determination of the Significant Factors of the Grouser Effect

To further determine the degree of the influence of the grouser's parameters on the traction force in the crawler robot's walking mechanism and based on the analysis and selection of the simulation experiment results and the need to determine the optimal performance of the grouser's parameters, a model of the process of the simulated experimental system was constructed. To further determine the significant factors affecting the traction force of the crawler robot, a cause-and-effect was is drawn based on Equations (9)–(14), as shown in Figure 8.

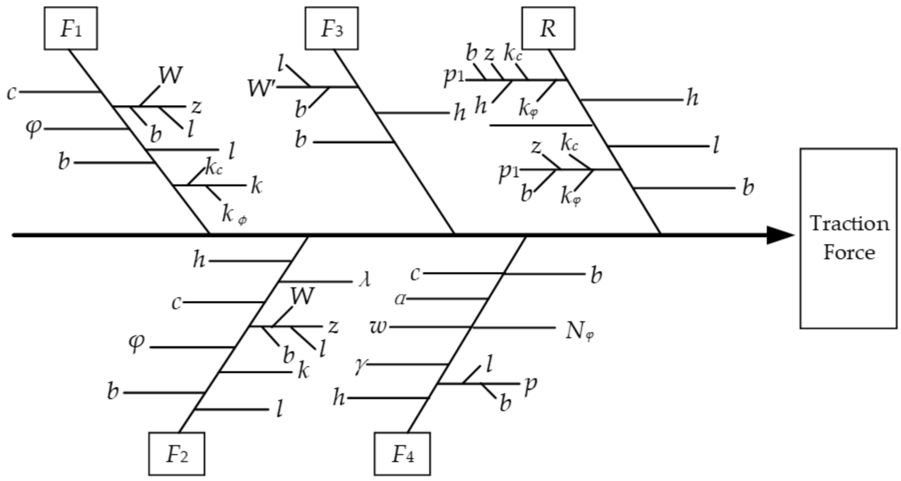

Figure 8. Causal analysis diagram of the traction force.

Through an analysis of Figure 8, it can be seen that the vertical thrust F_1 acting on the surface of the track shoe, the force F_2 acting on the bottom of the grouser, the force F_3 acting on both sides of the track shoe and the grouser, and the force F_4 acting on the grouser and the bulldozing resistance R collectively affects the hitch pull. Through an in-depth analysis, it was found that the parameters related to the crawler such as b, l, W, h, and λ, and soil parameters such as k_c, k_φ, γ, and N_φ have a major impact on the traction force. Among these, the moving speed of the robot and the track's parameters are controllable factors, but the soil parameters are uncontrollable factors. The traction process model in Figure 9 was obtained.

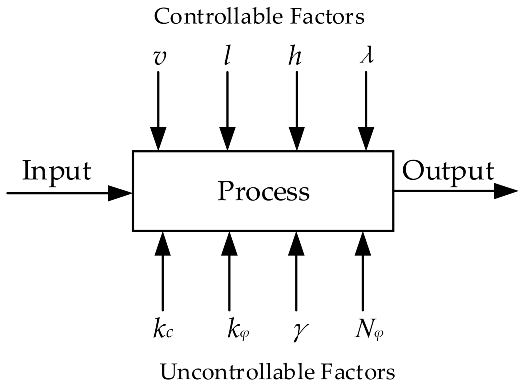

Figure 9. The traction process model.

4.2. Construction of the Dynamic Simulation Model

We used RecurDyn V9R3 software to build a mobile robot model and set up a smooth road surface, as shown in Figure 10. Since this section mainly examined the relationship between the controllable factors shown in Figure 9 and the traction force, a model of the reconfigurable wheel-crawler integrated walking mechanism in triangular crawler mode only was constructed, as shown in Figure 11. The parameters of the main components are shown in Table 1. Here, a compression spring device was arranged under the driving gear to ensure the real-time meshing of the driving wheel and the track. The track shoes could be modified according to the different parameters required for the test. It should be noted that to ensure the accuracy of the simulation, for track shoes of different widths, it is necessary to set different car body weights so that the force of the track shoes is the same.

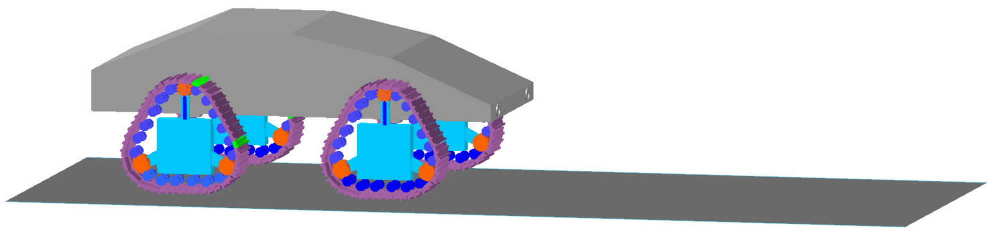

Figure 10. Model of the reconfigurable wheel-crawler robot.

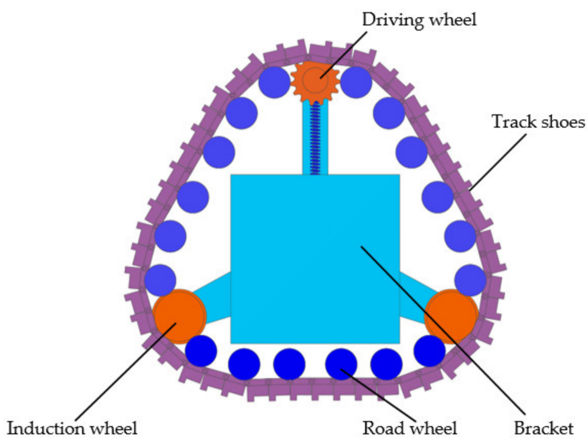

Figure 11. Triangular crawler mode of the walking mechanism.

Combining the terrain characteristics of the Qinghai–Tibet Plateau and the ground parameters of the road, the soil parameters of the simulated road surface were set as shown in Table 2.

Table 1. Parameters of the main components of the walking mechanism.

Component	Quantity	Parameters	
		Number of Teeth	15
Driving wheel	1	Base Circle Radius/mm	21.3844
		Pitch Circle Radius/mm	22.3844
		Inner Flange Radius/mm	26
		Wheel Radius/mm	23.5
Induction wheel	2	Inner Flange Width/mm	35
		Total Width/mm	45
		Wheel and Hub Width/mm	50
Road wheel	12	Wheel Radius/mm	13
		Hub Width/mm	30
		Pin Radius/mm	1.65
		Track Link Left Length/mm	13
Track shoes	Determined by width	Left Pin Height/mm	−10.2, 3
		Track Link Height/mm	6
		Grouser Width/mm	129

Table 2. Parameters of the soil pavement.

Definitions	Parameters
Terrain Stiffness (k_c)/kN·m$^{-(n+1)}$	3.7389×10^{-2}
Terrain Stiffness (k_φ)/kN·m$^{-(n+1)}$	1.0425×10^{-2}
Exponential Number (n)	1.1
Cohesion (c)/kPa	3.3×10^{-3}
Shearing Resistance Angle/°	33.7
Shearing Deformation Modulus/MPa	25
Sinkage Ratio	1.9×10^{-2}

4.3. Design of the Simulation Experiment

4.3.1. The Full Factorial Experimental Design

According to the structure of the reconfigurable wheel-crawler integration walking mechanism designed above, the track shoe's length was determined to be 129 mm. According to the research results of Xu Zhiyong, it was determined that the ratio of the thickness of the rectangular grouser to the length of the track shoe should be between 0.1 and 0.3, so the parameter $\lambda \in [0.1, 0.3]$ was determined. Since the ratio of the grouser's height to the track shoe's width is rarely more than 0.2 in practice, the grouser's height was set to 5 mm to 25.6 mm, according to the design formula for the track shoe's pitch

$$l = (1.75 \sim 2.3)\sqrt[4]{G}$$

where G is the total weight of the robot itself and the load.

Because of the combination of its weight and the design load of the reconfigurable wheel-crawler robot, the track pitch l was selected to be 12 mm to 20 mm. The maximum speed of the robot is 3 km/h. When the robot moves in the triangular crawler mode, the driving mode is changed from the direct drive of the main shaft to the main shaft driving the chain to the driving wheel, and the driving wheel is used to drive the track. Affected by the size of the driving wheel, the maximum moving speed of the robot is 0.893 km/h in the triangular track mode. In order to ensure the quality of the test, 20% and 60% of the maximum moving speed are respectively selected as the minimum moving speed and the maximum moving speed of the simulation test, which are about 0.18 km/h and 0.54 km/h.

To further study the effects of four parameters, namely the track shoe's pitch l, the grouser's height h, the ratio λ of the grouser's thickness to the track shoe's length, and the moving speed v of the crawler robot, on the traction of the track shoe, a complete factorial test was designed according to the literature [24]. The response quantities were l, h, λ, and v, and the three levels of the variables (low, medium, and high) are represented by −1, 0, and 1, respectively. The specific values assigned are shown in Table 3. To ensure the accuracy of the test, according to the horizontal distribution of the parameter λ, in this experiment, a track shoe with a width of 12 mm was used as a benchmark to carry a 100 kg car body. When the track shoe's width was 16 mm, the weight of the loaded car body was 42.3 kg. When the track shoe's width was 20 mm, the weight of the loaded car body was 27.5 kg. The test setup was constructed as shown in Table 4, and in the Modle −, + and 0 represent the parameter values corresponding to parameters −1, 1 and 0 in Table 3 respectively. The data obtained from the simulation test is also given in the Table 4.

Table 3. Response levels of the four parameters.

Response	Parameters		
	−1	**0**	**1**
λ	0.1	0.2	0.3
h	5	15.3	25.6
l	12	16	20
v	0.18	0.36	0.54

Table 4. The full factorial experimental design.

No.	Model	λ	h	l	v	FX
1	−−−−	0.1	5	12	0.18	47.04
2	−−−+	0.1	5	12	0.54	24.25
3	−−+−	0.1	5	20	0.18	32.9
4	−−++	0.1	5	20	0.54	23.55
5	−+−−	0.1	25.6	12	0.18	183.92
6	−+−+	0.1	25.6	12	0.54	180.94
7	−++−	0.1	25.6	20	0.18	151.34
8	−+++	0.1	25.6	20	0.54	149.58
9	0000	0.2	15.3	16	0.36	72.94
10	0000	0.2	15.3	16	0.36	72.94
11	0000	0.2	15.3	16	0.36	72.94
12	+−−−	0.3	5	12	0.18	44.23
13	+−−+	0.3	5	12	0.54	64.07
14	+−+−	0.3	5	20	0.18	29.92
15	+−++	0.3	5	20	0.54	23.94
16	++−−	0.3	25.6	12	0.18	168.33
17	++−+	0.3	25.6	12	0.54	113.91
18	+++−	0.3	25.6	20	0.18	107.56
19	++++	0.3	25.6	20	0.54	107

Through calculation, it can be seen that the ratios of the track shoe's pitch l, the grouser height's h, and the grouser's thickness to the track shoe's length λ were significant, while the moving speed v of the crawler robot was not significant. In light of the existing results, another response surface analysis was performed.

4.3.2. Response Surface Design Experiments

To improve the search for the optimal performance parameters within the above response range, and to conduct a more detailed analysis of all the significant factors, considering that there may be interactions among the parameters and that the model may also have curvature, the response surface design method was selected. The central review surface design (CCF) was used to optimize the design of the experimental program. Since the moving speed v of the crawler robot had no significant effect on the traction force, the moving speed of the robot was set to 0.18 km/h. The design of the experimental scheme is shown in Table 5, and in the Modle −, + and 0 represent the parameter values corresponding to parameters −1, 1 and 0 in Table 3 respectively. A and a correspond to parameter values of 1 and −1. The data obtained from the simulation test are also given in the Table 5.

Table 5. The response surface experimental design.

No.	Model	λ	h	l	FX
1	−−−	0.1	5	12	47.04
2	−−+	0.1	5	20	32.9
3	a00	0.1	15.3	16	83.31
4	−+−	0.1	25.6	12	183.92
5	−++	0.1	25.6	20	151.34
6	0a0	0.2	5	16	48.56
7	00a	0.2	15.3	12	86.52
8	000	0.2	15.3	16	84.36
9	000	0.2	15.3	16	84.36
10	000	0.2	15.3	16	84.36
11	000	0.2	15.3	16	84.36
12	000	0.2	15.3	16	84.36
13	000	0.2	15.3	16	84.36
14	00A	0.2	15.3	20	80.05
15	0A0	0.2	25.6	16	154.4
16	+−−	0.3	5	12	44.23
17	+−+	0.3	5	20	29.92
18	A00	0.3	15.3	16	92.52
19	++−	0.3	25.6	12	168.33

5. Simulation Test of the Grouser Effect

5.1. Establishment of the Regression Equation of the Grouser Effect

By observing the experimental data, we determined whether there was a singularity and deleted it. The combination of the data obtained from the response surface test in Table 4, the graphical summary chart shown in Figure 12, and the summary statistics shown in Table 6, it can be seen that the state of the data was relatively stable.

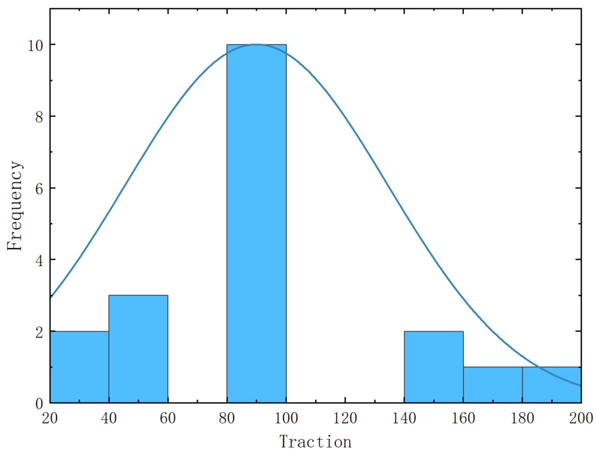

Figure 12. Graphical summary of the traction.

According to the output results in Table 6 that were used to verify the model, the R^2 was 0.982 and the adjusted R^2 was about 0.966, indicating that the output data were good. Among these statistics, the p-values of the response values of the grouser's height h, the grouser's pitch l, h^2, $h \times l$ and $\lambda \times h$ were all less than 0.05, indicating that these parameters were significant. The p-values of $\lambda \times l$, l^2, and λ^2 were all greater than 0.05, indicating that these parameters were not significant and needed to be optimized. For the ratio λ of the grouser's thickness to the length of the track shoe, the p-value was 0.0524, which is greater than 0.05, but since this response exists in the corresponding interaction λ*h, λ must be retained, marked with ˆ. In summary, the factors with significant correlation in ANOVA were marked with * in Table 7.

Table 6. Summary statistics.

Definitions	Parameters
Average	90.838
Standard deviation	45.553742
Mean standard error	9.7389129
95% upper limit of the mean	111.22178
95% lower limit of the mean	70.454211
Number	20
Number of missing values	0

Table 7. Parameter estimates and ANOVA table for the model.

Definitions	Estimated Value	Standard Error	T	p	Sig.
Intercept	85.568	2.764663	20.95	<0.0001	*
h	56.29	2.54312	22.13	0.00000	*
l	−12.827	2.54312	−5.04	0.00050	*
$h \times h$	−3.545	2.843294	−1.25	0.01563	*
$h \times l$	−4.095	4.849539	−0.84	0.01716	*
$\lambda \times h$	0.535	4.849539	0.11	0.04026	*
λ	−5.595	2.54312	−2.20	0.05244 ˆ	*
$\lambda \times l$	14.1	4.849539	2.91	0.24089	
$l \times l$	−8.1125	2.843294	−2.85	0.41818	
$\lambda \times \lambda$	−6.6975	2.843294	−2.36	0.91434	
S = 8.0421	R^2 = 0.982056	Adjustment R^2 = 0.965906		*R-sq.* (predict) = 80.28%	

The fitting model of the experimental data was optimized, the insignificant parameters were eliminated according to the analysis above, and the simplified model was finally obtained. As mentioned in the previous section, in the process of simplifying the model, the ordering principle needed to be followed. If a certain interaction effect in the parameters in the estimation is significant, the items that make up the interaction effect must be retained in the model. Table 8 shows the parameter estimates and variance analysis obtained after removing the insignificant items from the model. After the deletion of the insignificant items, both S and R^2 decreased because of the reduction in the number of items in the model, but the difference between R^2 and the adjusted R^2 was smaller. At the same time, the measured value and predicted value of the traction force were compared, as shown in Figure 13; this also shows that the simplified regression model is better.

Table 8. Parameter estimates and ANOVA table for the reduced model.

Definitions	Estimated Value	Standard Error	T	p
Intercept	84.856	2.475419	34.28	<0.0001
h	56.29	2.475419	22.74	0.00000
l	−12.827	2.475419	−5.18	0.00018
$h \times h$	11.964	3.500771	3.42	0.00459
$h \times l$	−8.1125	2.767602	−2.93	0.01169
$\lambda \times h$	−6.6975	2.767602	−2.42	0.03091
λ	84.856	2.475419	−2.26	0.04161
S = 7.828	R^2 = 0.97898	Adjustment R^2 = 0.967697	*R-sq.* (predict) = 90.84%	

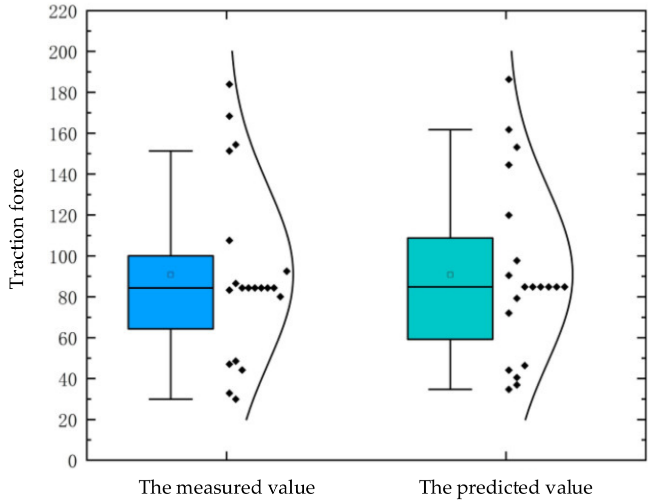

Figure 13. Normal comparison chart of the measured values and the predicted values of traction.

According to the different status of the data residuals after simplification of the model, it was determined whether the constructed model was normal. In Figure 14a, the residuals' scatter points are irregularly distributed, and there is no special funnel shape or trumpet shape, so it can be judged that the fitting model of the response is normal. By analyzing the normal distribution of the residual, the p-value was 0.161, which is greater than 0.05, the residuals conform to a normal distribution, as shown in Figure 14b [25].

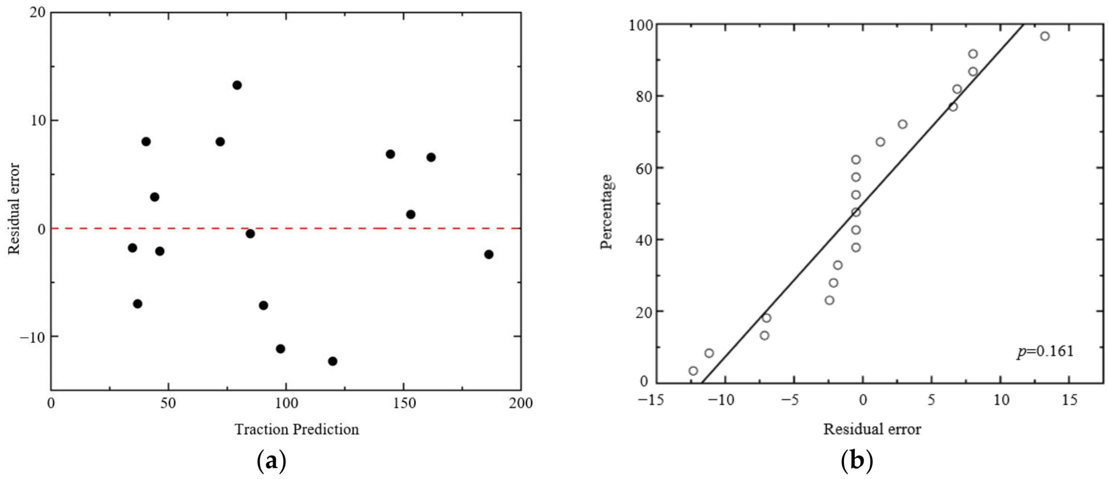

Figure 14. Analysis of residual error. (**a**) Scatterplot of the predicted values versus the residuals; (**b**) normal probability plot.

By observing whether the scatterplot of the residual error and each response was curved, we could judge whether the model was abnormal. In Figure 15, the scatter diagram of the residual error and the response values of the grouser's height h, the track shoe's pitch l, and the ratio λ of the grouser's thickness to the track shoe's length shows that a normal graph, and thus the model was determined to be normal.

The regression equation constructed for the measured traction force data is

$$\begin{aligned} FX_1 = {} & 85.568 - 5.595\lambda_1 + 56.29h_1 - 12.827l_1 \\ & -6.6975\lambda_1 h_1 - 3.545\lambda_1 l_1 - h_1 l_1 \\ & +0.531\lambda_1^2 + 14.1h_1^2 - 4.095l_1^2 \end{aligned} \tag{15}$$

where

$$\lambda_1 = \frac{\lambda - 0.2}{0.1},\ \lambda \in [0.1,\ 0.3]$$
$$h_1 = \frac{h - 15.3}{10.3},\ h \in [5,\ 25.6]$$
$$l_1 = \frac{l - 16}{4},\ l \in [12,\ 20]$$

After optimization of each response, the regression equation constructed from the predicted traction data is

$$\begin{aligned} FX_2 = {} & 84.856 - 5.595\lambda_1 + 56.29h_1 - 12.827l_1 \\ & -6.6975\lambda_1 h_1 - 8.1125h_1 l_1 + 11.964h_1^2 \end{aligned} \tag{16}$$

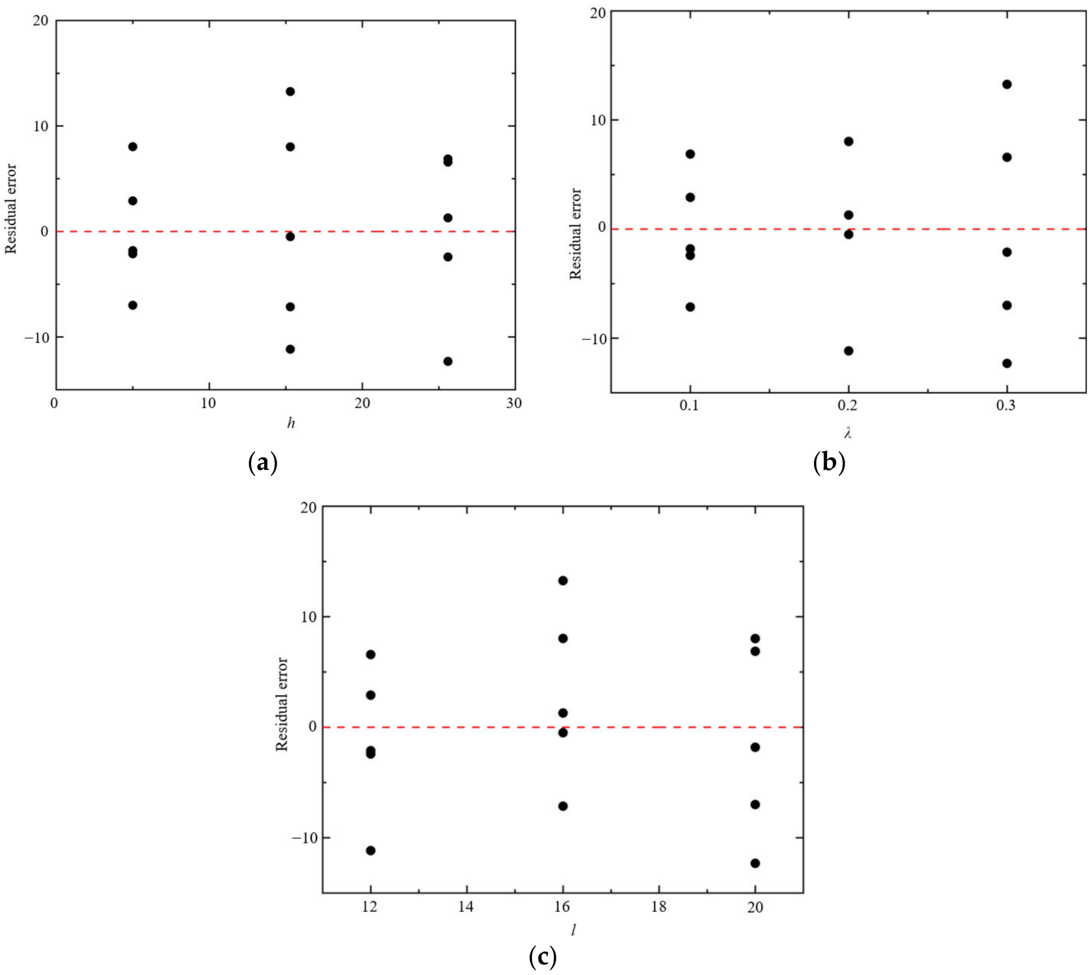

Figure 15. Scatterplot of the residuals vs. responses. (**a**) Scatterplot of the residuals vs. h; (**b**) scatterplot of the residuals vs. l; (**c**) scatterplot of the residuals vs. λ.

5.2. Coupling Analysis of Multiple Factors

After a reliable mathematical model had been created and its statistical significance had been confirmed, the effect of each input parameter on the traction force was estimated [26]. Figure 16 indicates the linear dependence of the traction force on all input parameters. The significance of $h \times h$, $h \times l$ and $\lambda \times h$ suggests a quadratic relation among the traction force but with smaller effects (3.41753, 2.93124 and 2.41996, respectively). Regarding the impact of individual factors, the grouser's height h has the strongest influence on the traction force (22.7396), the grouser's pitch l and the ratio of the grouser's thickness to the length of the track shoe λ have less influence on the traction force, which are 5.18175 and 2.26022, respectively.

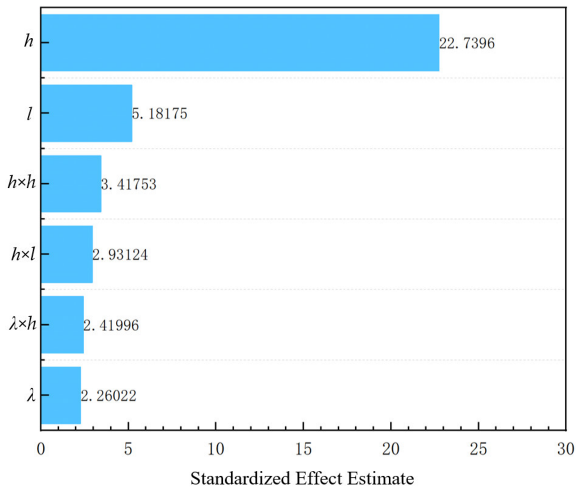

Figure 16. Pareto chart of standardized factor effects.

Figure 17 shows the effects of the interaction between the grouser's height and the track shoe's pitch on the traction force. When the grouser's height remained constant, the traction force gradually decreased with an increase in the track shoe's pitch. When the track shoe's pitch remained constant, the traction force gradually increased with an increase in the grouser's height. When the grouser's height and the track shoe's pitch changed at the same time, the growth rate of the traction force also showed a great change. When the track shoe's pitch was small, the traction force increased faster with an increase in the grouser's height. When the track shoe's pitch was large, the traction force increased slowly with an increase in the grouser's height. When the grouser's height was low, the traction force increased at a slower rate as the track shoe's pitch decreased. When the height of the grouser was large, the traction force increased faster with a decrease in the track shoe's pitch. It can be seen that the interaction between the grouser's height and the track shoe's pitch was more significant.

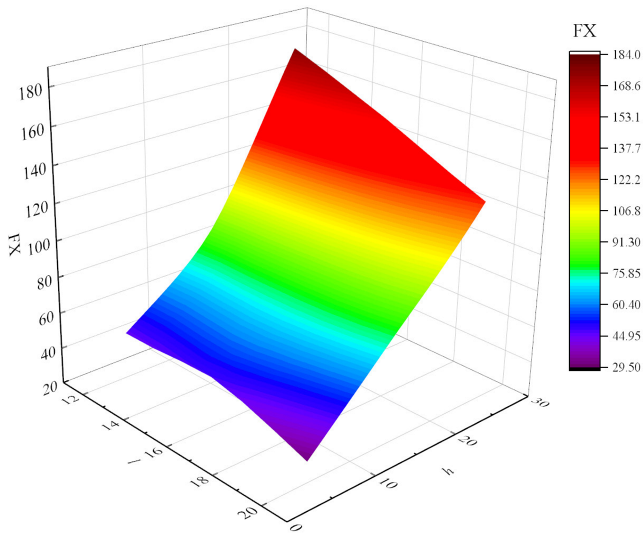

Figure 17. Effects of h and l on traction.

The p-values of $\lambda \times l$ were 0.24089, which is greater than 0.05, indicating that the parameter was not significant. Figure 18 shows the effects of the interaction between the ratio of the thickness of the grouser to the length of the track shoe λ and the pitch of the track shoe on the traction force. When λ was kept constant, the traction force gradually increased with a decrease in the track shoe's pitch. When the track shoe's pitch was kept constant, the traction force first gradually decreased and then increased as λ decreased.

When λ and the track shoe's pitch changed simultaneously, the change in the traction force was similar to the case of considering one response alone, and the change in traction force as a whole was not large. Therefore, it is verified that the interaction between the ratio λ of the thickness of the grouser to the length of the track shoe and the pitch of the track shoe was not significant.

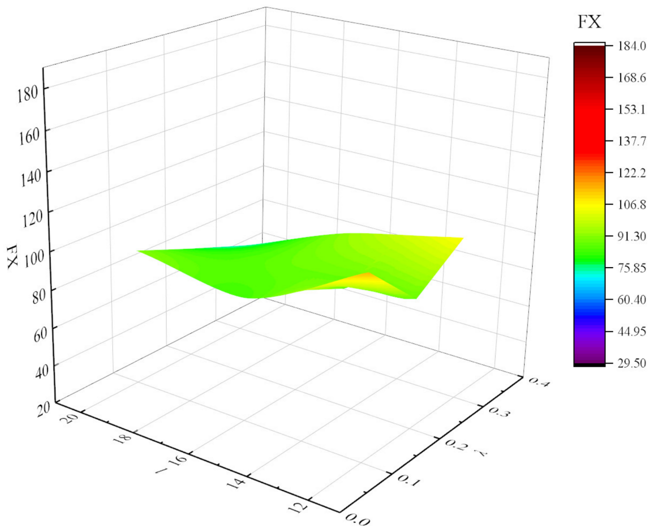

Figure 18. Effects of λ and l on traction.

Figure 19 shows the effects of the interaction between the ratio of the thickness of the grouser to the length of the track shoe λ and the height of the grouser on the traction. When λ remained constant, the traction force gradually increased with an increase in the grouser's height. When the grouser's height h remained constant, the traction force gradually increased with a decrease in λ. When λ and the grouser's height h changed at the same time, the growth rate of the traction force changed greatly. When λ was small, the traction force increased faster as the grouser's height h increased. When λ was large, the traction force increased slowly with an increase in the grouser's height. When the grouser's height was small, the traction force increased slowly with a decrease in λ. When the grouser's height h was larger, the traction force increased faster with an increase in λ. It can be seen that the interaction between the ratio of the thickness of the grouser to the length of the track shoe λ and the height of the grouser h was more significant.

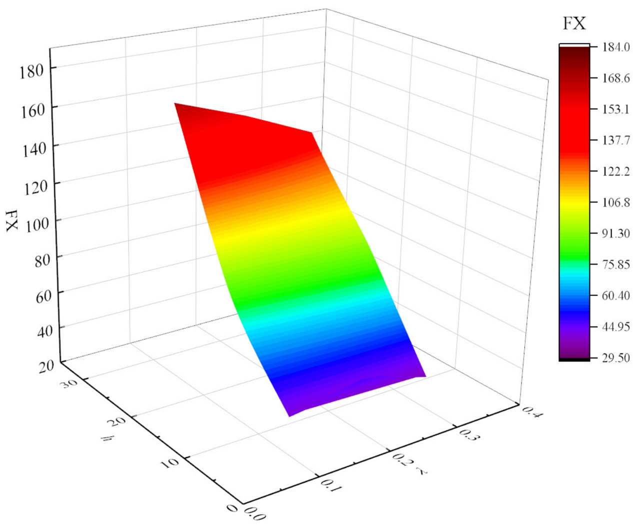

Figure 19. Influence of λ and h on the traction force.

Through the above analysis, combined with Equation (16), it can be seen that when the traction force on the track shoe was selected to take the maximum value within the test range, the ratio λ of the thickness of the grouser to the length of the track shoe was 0.1, and the height h of the track shoe was 25.6 mm. The distance l was 12 mm. A simulation test was carried out according to these parameters, and the traction force on the track shoe was 179.73 N, as shown in Figure 20.

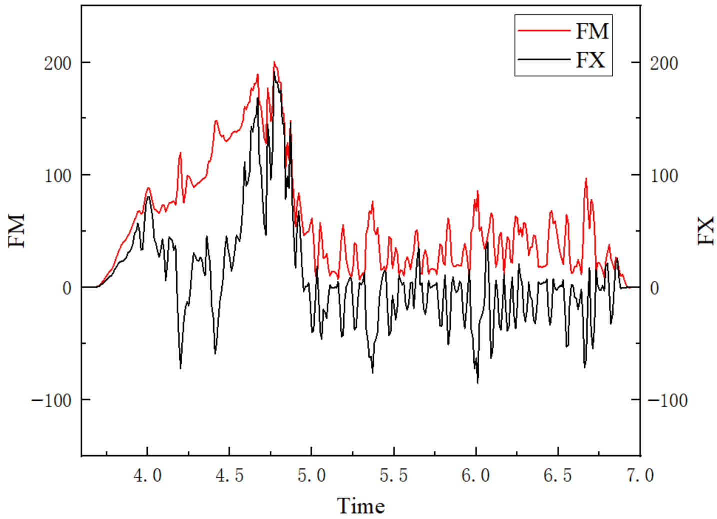

Figure 20. Simulation curve of maximum traction.

In Figure 20, the red curve is the overall force curve of the track shoe, and the black curve is the curve of the traction force on the track shoe. From the time when the grouser came into contact with the soil, the track shoe began to be affected by the traction force, and the traction force gradually increased as the contact angle with the soil increased. When the grouser was perpendicular to the road's soil, the traction dropped rapidly. As the traveling mechanism advanced, the traction force on the track shoes fluctuated up and down on the X-axis and was mainly based on the force opposite the driving direction. The main reason for this situation is that the track shoes that engage with the soil successively behind this track shoe provided greater traction, which created a pulling force on the front track shoe. In addition, it can be seen from Figure 18 that the traction force on the track shoes fluctuated greatly during the simulation process; the main reason for this was that the grouser was too high and thin. Although the response parameters determined by the tests above obtained the maximum traction force, at the same time, they also produced an unfavorable effect of unstable motion.

6. Conclusions

This study systematically analyzed the grouser effect when the mechanism operated in triangular track mode and conducted a dynamic simulation test design based on the surface response. According to the experimental results, a prediction model for the grouser effect of the reconfigurable wheel-crawler integrated walking mechanism under the triangular crawler mode is established. The results of the analysis show that the traction force is dependent on the input parameters, including the ratio λ of the grouser's thickness to the length of the track shoe, the grouser's height h, the grouser's pitch l, $h \times h$, $h \times l$, and $\lambda \times h$. And the grouser's height h has the greatest influence on the traction force. Through the coupling analysis of λ, h and l, the significance of the influence of $h \times l$, and $\lambda \times h$ on the traction force is further verified. When the traction force on the track shoe was selected to take the maximum value within the test range, the ratio λ of the thickness of the grouser to the length of the track shoe was 0.1, and the height h of the track shoe was 25.6 mm. The distance l was 12 mm.

In this paper, the method of response surface is used to carry out the simulation test of the grouser effect, and reliable results can be obtained with a small number of experiments. The prediction equation proposed in the current analysis represents the basic model of the grouser effect in the triangular crawler mode of the reconfigurable wheel-crawler integrated walking mechanism. In this direction, it is necessary to further analyze the wheel-terrain mechanics model of the crawler parameters on the outer side of the track in the wheel mode, and comprehensively analyze and determine the parameters of the grouser. In that case, the reconfigurable wheel-crawler integrated walking mechanism can obtain better ground adaptability in both the circular wheel mode and the triangular crawler mode.

Supplementary Materials: The following supporting information can be downloaded at: www.bilibili.com/video/BV17y4y1d7ER/?spm_id_from=333.999.0.0.&vd_source=4097b7d60217d63e0d402d3e6c676c1a (accessed on 22 January 2022).

Author Contributions: Methodology, S.T.; software, P.Z.; validation, P.Z., S.T. and Z.S.; writing—original draft preparation, P.Z.; writing—review and editing, S.T. and Z.S.; supervision, Z.S.; project administration, S.T. All authors have read and agreed to the published version of the manuscript.

Funding: This work was supported by the Key Technology Research Program of Inner Mongolia (Grant No. 2021GG0258), the Natural Science Foundation of Inner Mongolia (Grant No. 2021MS05005), the National Key R&D Program of China (Grant No. 2018YFB1307501), the National Natural Science Foundation of China (Grant No. 61763036), the Program for Innovative Research Team in Universities of the Inner Mongolia Autonomous Region (Grant No. NMGIRT2213), the Fundamental Research Funds for the directly affiliated Universities of Inner Mongolia Autonomous Region (Grant No. JY20220046). This support is gratefully acknowledged by the authors.

Institutional Review Board Statement: Not applicable.

Informed Consent Statement: Not applicable.

Data Availability Statement: Not applicable.

Conflicts of Interest: The authors declare no conflict of interest.

References

1. Bai, Y.; Sun, L.; Zhang, M.; Liu, X.; Li, Z. Progress of research on terramechanics for tracked mobile robots. *Mech. Des.* **2020**, *10*, 1–13. [CrossRef]
2. Bekker, M.G. *Theory of Land Locomotion*; The Univ. of Michigan Press: Ann Arbor, MI, USA, 1956.
3. Bekker, M.G. *Off-Road Locomotion: Research and Development in Terramechanics*; The Univ. of Michigan Press: Ann Arbor, MI, USA, 1960.
4. Xiao, W.; Zhang, Y. Design of Wheel of Manned Lunar Rover and Research on Terramechanics Model for Wheel-Terrain Interaction Based on Elastic Wheel. *J. Mech. Eng.* **2016**, *10*, 119–125. [CrossRef]
5. Wismer, R.D.; Luth, H.J. Off-road traction prediction for wheeled vehicles. *J. Terramech.* **1974**, *10*, 49–61. [CrossRef]
6. Wong, J.-Y.; Reece, A.R. Prediction of rigid wheel performance based on the analysis of soil-wheel stresses part I. Performance of driven rigid wheels. *J. Terramech.* **1967**, *4*, 81–98. [CrossRef]
7. Bekker, M.G. Mechanics of off-the-road locomotion. *Proc. Inst. Mech. Eng. Automob. Div.* **1962**, *16*, 25–44. [CrossRef]
8. Liang, D.; Deng, Z.; Gao, H.; Tao, J.; Iagnemma, K.D.; Liu, G. Interaction mechanics model for rigid driving wheels of planetary rovers moving on sandy terrain with consideration of multiple physical effects. *J. Field Robot.* **2015**, *32*, 827–859. [CrossRef]
9. Guo, J.; Li, W.; Gao, H.; Ding, L.; Deng, Z. In-situ wheel sinkage estimation under high slip conditions for grouser-wheeled planetary rovers: Another immobility index. *Mech. Mach. Theory* **2021**, *158*, 104243. [CrossRef]
10. Yang, C.B.; Gu, L.; Lv, W.W. Study of Factors with Effects on Tracked Vehicle Driving Resistance Basis of Bekker Theory. *Appl. Mech. Mater.* **2013**, *288*, 80–83. [CrossRef]
11. Yang, C.B.; Gu, L.; Li, Q. Finite element simulation of Track shoe and Ground adhesion. *Appl. Mech. Mater.* **2014**, *644–650*, 402–405. [CrossRef]
12. Yang, C.; Cai, L.; Liu, Z.; Tian, Y.; Zhang, C. A calculation method of track shoe thrust on soft ground for splayed grouser. *J. Terramech.* **2016**, *65*, 38–48. [CrossRef]
13. Yokoyama, A.; Nakashima, H.; Shimizu, H.; Miyasaka, J.; Ohdoi, K. Effect of open spaces between grousers on the gross traction of a track shoe for lightweight vehicles analyzed using 2d dem. *J. Terramech.* **2019**, *90*, 31–40. [CrossRef]
14. Li, J.; Bie, E.; Wu, Z.; Jin, S.; He, J. Research on Maximum Traction Characteristics of 3D Model of Track Shoe-Soil. *Agric. Equip. Veh. Eng.* **2016**, *57*, 6. [CrossRef]
15. Li, J.; Li, Q.; Zhou, J.; Zhang, Y.; Xie, C. Analysis of Track-Terrain Interaction on Soft Soil. *Acta Armament.* **2012**, *12*, 1423–1429.

16. Gan, L.; Huang, Q.; Chen, S. Study on Design and Traction Performance of Ostrich-foot Sandy Track Shoe. *Mech. Sci. Technol. Aerosp. Eng.* **2022**, *41*, 673–680.
17. Xu, Z.; Liu, Y.; Yang, G.; Xia, J.; Dou, Z.; Meng, Q.; Xu, X. Research on contact model of track-soft sediment and traction performance of four-tracked seabed mining vehicle. *Ocean Eng.* **2022**, *259*, 111902. [CrossRef]
18. Yang, C.B.; Dong, M.M.; Gu, L.; Li, Q.; Gao, X.D. Research on soil shear strength considering the shape of grouser. *Trans. Beijing Inst. Technol.* **2015**, *35*, 1118–1121. [CrossRef]
19. Li, J.; Sun, S.; Peng, J. Experimental Study on Effect of Structural Parameters of Track Shoe on Traction Force. *Agric. Equip. Veh. Eng.* **2015**, *55*, 15–18.
20. Chen, Z.; Xue, D.; Wang, G.; Cui, D.; Fang, Y.; Wang, S. Simulation and optimization of the tracked chassis performance of electric shovel based on DEM-MBD. *Powder Technol.* **2021**, *390*, 428–441. [CrossRef]
21. Zhou, L.; Gao, J.; Hu, C.; Li, Q. Numerical simulation and testing verification of the interaction between track and sandy ground based on discrete element method. *J. Terramech.* **2021**, *95*, 73–88. [CrossRef]
22. Yang, K.; Gan, L.; Chen, S.; Xu, X.; Sun, X.; Zhou, Q.; Jiang, X.; Hu, D.; Liu, D.; Wang, Z. Research on the design and traction characteristics of a vehicle track shoe for sandy land. *Proc. Inst. Mech. Eng. Part C J. Mech. Eng. Sci.* **2022**, *236*, 5826–5835. [CrossRef]
23. Taghinezhad, J.; Alimardani, R.; Masdari, M.; Mahmoodi, E. Performance optimization of a dual-rotor ducted wind turbine by using response surface method. *Energy Convers. Manag. X* **2021**, *12*, 100120. [CrossRef]
24. Ahmed, M.; Ayub, A.; Sheikh, N.A.; Shahzad, M.W.; Haroon, M.; Imran, M. Thermodynamic optimization and performance study of supercritical CO_2 thermodynamic power cycles with dry cooling using response surface method. *Int. Commun. Heat Mass Transf.* **2023**, *142*, 106675. [CrossRef]
25. Kostić, S.; Vasović, N.; Sunarić, D. Slope stability analysis based on experimental design. *Int. J. Geomech.* **2016**, *16*, 3–36. [CrossRef]
26. Kostić, S.; Vasović, N.; Marinković, B. Robust optimization of concrete strength estimation using response surface methodology and Monte Carlo simulation. *Eng. Optim.* **2017**, *49*, 864–877. [CrossRef]